Liquid Crystals
Publication details, including instructions for authors and subscription information:
http://www.informaworld.com/smpp/title~content=t713926090

Crossed fields induced periodic deformations in nematics: Effect of weak anchoring

U. D. Kini[a]
[a] Raman Research Institute, Bangalore, India

To cite this Article Kini, U. D.(1996) 'Crossed fields induced periodic deformations in nematics: Effect of weak anchoring', Liquid Crystals, 21: 5, 713 — 726
To link to this Article: DOI: 10.1080/02678299608032883
URL: http://dx.doi.org/10.1080/02678299608032883

LIQUID CRYSTALS, 1996, VOL. 21, NO. 5, 713–726

Crossed fields induced periodic deformations in nematics: effect of weak anchoring

by U. D. KINI†
Raman Research Institute, Bangalore-560080, India

(*Received 9 January 1996; in final form 23 May 1996; accepted 24 May 1996*)

Theoretical studies are reported on the formation of static periodic distortions (PD) in a homeotropically aligned nematic insulator under the action of crossed electric (**E**) and magnetic (**H**) fields impressed in the sample plane. Linear stability analysis is used along with the Rapini–Papoular expression for surface free energy. Depending upon the material parameters, the direction of periodicity as well as the stripe width may change continuously or discontinuously with variation of the angle between **H** and **E**. The strength of director anchoring influences the phase diagrams as well as the nature of the transition between different distortion states. Curiously, some of the phase diagrams resemble those calculated recently for a thermotropic transition.

1. Introduction

Many interesting effects result from the application of **E** and **H** fields on nematic samples. These have been satisfactorily explained by the continuum theory [1–4]. For instance, a periodic distortion (PD) associated with wavevector of periodicity in the sample plane can be caused by impressing **H** on samples with high elastic anisotropy [5, 6]. Due to the presence of flexoelectricity [7], PD is known to be formed under the action of a static **E** field [8] even in nematics with moderate elastic anisotropy. A time varying **E** field is also known to cause PD [9]. Effects of **E** are generally more interesting and more complex than those of **H** because director deformations can modify the **E** field inside the sample [10]. A number of theoretical studies have been reported [11] to account for the above observations and to study possible effects of director boundary tilt and director anchoring [12] on the formation of PD in nematics.

The joint application of **H** and **E** along two mutually perpendicular directions (called the *crossed field configuration*) has led to the observation of a first order Freedericksz transition [13, 14] as well as field induced biaxiality [14–16]. PD has also been reported [14, 15] in a material (5CB) with positive dielectric and diamagnetic anisotropies ($\varepsilon_A > 0$; $\chi_A > 0$; [17]). The studies of [13–15] pertain to initial homeotropic director tilt with **E** being impressed in the sample plane, parallel to the sample boundaries; **H** is the stabilizing field applied normal to the plates. Attempts have been made to explain the occurrence of PD [14, 15] on the basis of non-linear as well as linear perturbation theory [18, 19]. It is shown [19] that PD can result due to the modification of **E** inside the sample caused by director field perturbations.

The linear perturbations approach of [19] has been recently extended [20] to study PD in homeotropically aligned samples of materials having different kinds of dielectric and diamagnetic anisotropy [21, 22] with **E** and **H** impressed in the sample plane. With the rigid anchoring hypothesis, it is shown that in a material such as M1 [21] with $\varepsilon_A < 0$ and $\chi_A > 0$, PD may result due to a destabilizing **H** acting in the plane of the sample; the direction of periodicity may change discontinuously for continuous variation of the angle (α) between **H** and **E**. In a material such as CCH-7 [22] ($\varepsilon_A > 0$ and $\chi_A < 0$), PD may be caused by the destabilizing **E** field acting against a stabilizing **H** and the direction of periodicity may change continuously with α. Phase diagrams have been drawn for different kinds of PD.

With the convenience of the rigid anchoring hypothesis, the analytically derived results can all be scaled to be independent of the sample thickness. In reality, a more complete picture of the director configurations will emerge only by including the finite surface free energy density [12]. With this, the sample thickness becomes a parameter in the problem and can be expected to influence the results via a change in the nature of scaling as well as a change in the size (if not the shape) of the phase diagrams for different instability Modes.

Theoretical results of [13–15, 18–20] pertain to a

†email address: udkini@rri.ernet.in

0267–8292/96 $12·00

nematic insulator whose electrical conductivity is assumed to be zero. Nematics have low conductivities and can be treated as insulators in many situations. But their conductivity anisotropy is considerable. In some materials, the application of **E** leads to electrohydrodynamic instabilities (EHD; [23]). Still, one can consider the possibility of static distortions through a modification of the applied **E** field caused by conductivity [24, 25]. The possible influence of conductivity on the formation of PD in crossed field configurations cannot be ruled out. Recent studies also show some exotic effects such as modification of director anchoring strength in nematics with ionic impurities [26].

With the above introduction, the motivation for the present work becomes clear. As a first step, the governing equations are set up for a nematic insulator weakly anchored at the boundaries (§2). Results for M1 and CCH-7 are presented in § 3 and § 4, respectively. Section 5 summarizes the conclusions with a brief discussion on the possible effects of conductivity.

2. Governing equations, boundary conditions

An insulating nematic sample of thickness $2h$ contained between glass plates $z = \pm h$ (glass is assumed to be an isotropic dielectric) is sandwiched between electrodes at $x = \pm g$ lying in the yz plane. The electrode gap $2g$ is large compared to the sample thickness $2h$ and the sample is studied near $x = 0$, midway between the electrodes. The nematic is initially oriented along z with the unit director field $\mathbf{n}_o = (0, 0, 1)$. The directions of the *free axes* at both plates are along z. The magnetic field is either along z, $\mathbf{H}_\parallel = (0, 0, H_\parallel)$ or in the xy plane, $\mathbf{H}_\perp = (H_\perp C_\alpha, H_\perp S_\alpha, 0)$; α is measured in radians. When $\alpha = 0$, $\mathbf{H}_\perp$ is along x, while for $\alpha = \pi/2$, it is along y. The unperturbed electric field $\mathbf{E}_o = (E_{xo}, 0, 0)$ inside the sample is uniform with $E_{xo} = V_o/2g$ where V_o is the potential difference applied between the electrodes. Under perturbations, the director and the **E** field become

$$\mathbf{n} = (\sin\theta, \cos\theta \sin\phi, \cos\theta\cos\phi);$$
$$\mathbf{E} = \mathbf{E}_o + \mathbf{E}'; \quad \mathbf{E}' = -\nabla\psi \tag{1}$$

where the perturbations θ, ϕ and ψ are functions of x, y and z; use of Maxwell's curl equation enables expression of the electric field perturbation as the gradient of the scalar potential ψ; a subscripted comma denotes partial differentiation. For linear perturbations, terms are retained to linear order in the governing equations and to second order in the free energy. At constant potential difference (V_o) between the electrodes [27], the total free energy F is written as the sum of the volume and surface terms,

$$F = \int_\Omega W_\Omega \mathrm{d}\Omega + A W_S(z = h) + A W_S(z = -h);$$
$$W_\Omega = \frac{K_1}{2}(\theta_{,x} + \phi_{,y})^2 + \frac{K_2}{2}(\phi_{,x} - \theta_{,y})^2 + \frac{K_3}{2}(\theta_{,z}^2 + \phi_{,z}^2)$$
$$- \frac{1}{8\pi}(\varepsilon_A E_{xo}^2\theta^2 - 2\varepsilon_A E_{xo}\theta\psi_{,z} + \varepsilon_\perp\psi_{,x}^2$$
$$+ \varepsilon_\perp\psi_{,y}^2 + \varepsilon_\parallel\psi_{,z}^2) + f_M;$$
$$W_S = \frac{B}{2}\theta^2 + \frac{B}{2}\phi^2;$$
$$f_M = -\frac{\chi_A H_\perp^2}{2}(C_\alpha\theta + S_\alpha\phi)^2 \text{ if } H_\parallel = 0 \text{ or}$$
$$f_M = \frac{\chi_A H_\parallel^2}{2}(\theta^2 + \phi^2) \text{ if } H_\perp = 0 \tag{2}$$

where Ω is the sample volume, A the area of each sample plane, W_Ω the volume free energy density, W_S the surface free energy density evaluated separately at the two plates; K_1, K_2, K_3 are, respectively, the splay, twist and bend elastic constants of the nematic; $S_\alpha = \sin\alpha$ and $C_\alpha = \cos\alpha$; the magnetic term f_M takes one of two values depending upon the direction of application of **H**; B is the polar anchoring strength at the two surfaces; $\varepsilon_A = \varepsilon_\parallel - \varepsilon_\perp$ where $\varepsilon_\parallel$ and $\varepsilon_\perp$ are, respectively, the dielectric constants along and normal to the nematic director. In the linear limit, the surface free energy is written as a term proportional to the square of the perturbation at the boundary (the perturbation gives the deviation of the director field away from the free axis). Terms corresponding to the surface elastic constants K_4 and K_{13} [1–4] have been ignored. Flexoelectricity [7] has also not been included. This may be a meaningful assumption if the applied **E** field is time varying with sufficiently high frequency.

Maxwell's divergence equation results by minimizing F with respect to ψ holding other quantities constant:

$$\varepsilon_A E_{xo}\theta_{,z} - \varepsilon_\perp\psi_{,xx} - \varepsilon_\perp\psi_{,yy} - \varepsilon_\parallel\psi_{,zz} = 0. \tag{3}$$

Interestingly, the modification of **E** inside the nematic is caused by θ and not ϕ. This is to be expected in the linear limit as ϕ lies in the yz plane, normal to $\mathbf{E}_o$. When ψ is held fixed and F minimized with respect to θ and ϕ, one finds

$$K_1\theta_{,xx} + K_2\theta_{,yy} + K_3\theta_{,zz} + \theta\left(\frac{\varepsilon_A E_{xo}^2}{4\pi} + a_\theta\right) + a_\phi\phi$$
$$+ (K_1 - K_2)\phi_{,xy} - \frac{\varepsilon_A E_{xo}}{4\pi}\psi_{,z} = 0. \tag{4}$$

$$K_2\phi_{,xx} + K_1\phi_{,yy} + K_3\phi_{,zz} + b_\phi\phi + b_\theta\theta + (K_1 - K_2)\theta_{,xy} = 0, \quad (5)$$

$$a_\theta = \chi_A H_\perp^2 C_\alpha^2 \text{ and } a_\phi = \chi_A H_\perp^2 S_\alpha C_\alpha;$$
$$\text{or } a_\theta = -\chi_A H_\parallel^2 \text{ and } a_\phi = 0;$$
$$b_\phi = \chi_A H_\perp^2 S_\alpha^2 \text{ and } b_\theta = \chi_A H_\perp^2 S_\alpha C_\alpha;$$
$$\text{or } b_\phi = -\chi_A H_\parallel^2 \text{ and } b_\theta = 0. \quad (6)$$

The boundary conditions resulting from this variation are

$$\pm K_3\theta_{,z} + B\theta = 0 \text{ at } z = \pm h,$$
$$\pm K_3\phi_{,z} + B\phi = 0 \text{ at } z = \pm h. \quad (7)$$

The condition on ψ is imposed by observing that $\mathbf{E}$ is always along x inside the glass plates (isotropic dielectrics). In the nematic, however, $\mathbf{E}$ is perturbed (1). At $z = \pm h$, the interfaces between two dielectrics, the normal component of the electric induction (D_z) should be continuous. In the glass plates, $D_z = 0$ as D should be along x. Hence, D_z should vanish at the two interfaces so that*

$$\varepsilon_A E_{xo}\theta - \varepsilon_\parallel \psi_{,z} = 0 \quad \text{at } z = \pm h. \quad (8)$$

Clearly, θ and ϕ will not vanish at the boundaries when the anchoring strength is finite. The next sections consider different solutions of the governing equations (3)–(6) with boundary conditions (7) and (8). Even in the most general case, this reduces to the solution of an eigenvalue problem. In any given case, depending upon the assumptions, a subset of terms from (3)–(5) is chosen for solution. E_{xo} can be assumed to be positive without loss of generality as the transformation $E_{xo} \to -E_{xo}$, $\theta \to -\theta$, $\phi \to -\phi$ leaves equations (3)–(8) unchanged. This is intuitively clear due to cylindrical symmetry in the xy plane about the unperturbed director $\mathbf{n}_o$. We assume that $H_\parallel = 0$ (except at the end of §4.1).

The threshold for the aperiodic or homogeneous deformation HD is deduced by assuming that the perturbations are functions of z alone. The material is assumed to have opposite signs of ε_A and χ_A (this is true of M1 [21] and CCH-7 [22]). In the general case, all three perturbations are present. We choose the solution with θ and ϕ symmetric and ψ antisymmetric relative to $z = 0$. The *ansatz* for perturbations is

$$(\theta, \phi, \psi) = \left(\theta_A \cos\frac{qz}{h}, \phi_A \cos\frac{qz}{h}, \psi_A \sin\frac{qz}{h}\right)$$

where θ_A, ϕ_A and ψ_A are constants whose absolute magnitudes are not known; only the ratio of any two of them can be found. We ignore the other solution (having higher threshold) in which the perturbations have the opposite spatial symmetry. Equation (3) integrates to satisfy (8) identically and enables substitution for $\psi_{,z}$ in terms of θ in (4). Solving (4) and (5) with (7), the compatibility condition for the HD threshold results,

$$q^4 - q^2(\sigma_H + \sigma_E) + \sigma_H\sigma_E S_\alpha^2;$$
$$\sigma_H = \frac{\chi_A h^2 H_\perp^2}{K_3}; \quad \sigma_E = \frac{\varepsilon_\perp \varepsilon_A h^2 E_{xo}^2}{4\pi K_3 \varepsilon_\parallel} \quad (9)$$

where q satisfies the condition,

$$\eta\cos q - q\sin q = 0; \quad \eta = \frac{Bh}{K_3}. \quad (10)$$

The dimensionless quantity η is the ratio between the semisample thickness h and the characteristic length K_3/B; η measures to what extent the anchoring at the surface can balance the volume elastic torque. Equation (10) is solved numerically to obtain q for a given value of η. When $\eta \gg 1$, $q \approx \pi/2$; when $\eta \to 0$, $q \to 0$. For a material such as M1 [21], the HD threshold H_F with a stabilizing $\mathbf{E}_o$ is found from (9) and (10):

$$H_F^2 = \frac{K_3 q^2(q^2 - \sigma_E)}{\chi_A h^2(q^2 - \sigma_E S_\alpha^2)}. \quad (11)$$

With (9) and (10), the HD threshold E_F for a material such as CCH-7 [22] with a stabilizing $\mathbf{H}_\perp$ is given by

$$E_F^2 = \frac{4\pi K_3 \varepsilon_\parallel q^2(q^2 - \sigma_H)}{\varepsilon_\perp \varepsilon_A h^2(q^2 - \sigma_H S_\alpha^2)}. \quad (12)$$

For strong anchoring, the expressions in (11) and (12) approach the corresponding ones of [20].

3. Material (M1) with $\varepsilon_A < 0$ and $\chi_A > 0$

$\mathbf{H}_\perp$ destabilizes the director orientation while $\mathbf{E}_o$ has a stabilizing action. The magnetic threshold for instability is studied as a function of E_{xo} and other parameters. When $\mathbf{E}_o$ alone is impressed, the cylindrical symmetry about $\mathbf{n}_o$ gets broken along only one direction, x. Once $\mathbf{H}_\perp$ is also present in the xy plane, the symmetry can be broken along yet another direction. Hence, three varieties of PD are studied—the xz Mode (periodicity along x and perturbations depending on x and z); the yz Mode (periodicity along y and perturbations depending on y and z); the xyz Mode (periodicity in the xy plane and perturbations depending on x, y and z). It is convenient to first of all discuss results for $\mathbf{H}_\perp$ acting along

* As pointed out in reference [20] (see note [26] and also §5 therein), we do not explicitly enforce the condition of continuity of the tangential components of $\mathbf{E}$ at the boundaries $z = \pm h$ separating the two dielectrics. Again, due to the tacit assumption of infinite extent of the sample along x and y, restrictions cannot be imposed on electric field perturbations E_x' and E_y' along the sample peripheries in the xz and yz planes. These constitute limitations of the calculations presented in this work noting especially that the voltage between electrodes is assumed to be unchanged at V_o under variations.

x ($\alpha = 0$). As α vanishes, the magnetic coupling term connecting θ and ϕ drops out of (4) and (5). This causes ϕ to damp out for both the xz and yz Modes. As both $\mathbf{E}_o$ and $\mathbf{H}_\perp$ break the cylindrical symmetry along the same direction, x and y become symmetry directions in the xy plane.

3.1. *Results for PD in M1 at $\alpha = 0$*

For the xz Mode, for instance, solutions are sought such that

$$(\theta, \psi) = \left(\theta_A \cos\frac{qz}{h}, \psi_A \sin\frac{qz}{h}\right) \sin\left(\frac{Q_x x}{h}\right)$$

where Q_x is a dimensionless wavevector corresponding to a wavelength $\lambda_x = 2\pi h/Q_x$. As $2g \gg 2h$, the sample is essentially unbounded along x. Q_x is not a function of coordinates but depends upon material and interfacial parameters. From (4), (5), (7) and (8) the following compatibility condition results:

$$\begin{aligned}
&(\cos q_1)[\eta(q_1^2 + p_2^2) + p_2(\tanh p_2)(p_2^2 - \beta_1 Q_x^2)] \\
&\quad - q_1(\sin q_1)(\beta_1 Q_x^2 + q_1^2) = 0; \\
&2q_1^2 = -X_1 + (X_1^2 + 4X_2)^{1/2}; \\
&2p_2^2 = X_1 + (X_1^2 + 4X_2)^{1/2}; \\
&X_1 = Q_x^2(\beta_1 + \gamma_1) - \sigma_H - \sigma_E; \\
&X_2 = Q_x^2(\beta_1\sigma_H + \sigma_E - \beta_1\gamma_1 Q_x^2); \\
&\beta_1 = \frac{\varepsilon_\perp}{\varepsilon_\parallel}; \quad \gamma_1 = \frac{K_1}{K_3}.
\end{aligned} \tag{13}$$

The only elastic constants associated with the xz Mode are K_3 and K_1. When $Q_x \to 0$, the condition in (13) tends to (10) corresponding to HD. To solve for the PD threshold, E_{xo} is fixed at a suitable value. With Q_x close to zero, the lowest value of $H_\perp$ satisfying (13) is found. When $Q_x \to 0$, $H_\perp(Q_x) \to H_F$ of (11). Variation of Q_x shows that $H_\perp(Q_x)$ diminishes with increase of Q_x reaching a minimum $H_{PX} = H_\perp(Q_{PX})$ at $Q_x = Q_{PX}$. H_{PX} is the xz Mode threshold and Q_{PX} the dimensionless wavevector at threshold; the dimensionless threshold for the xz Mode is

$$r_X = H_{PX}/H_F.$$

If $r_X < 1$, the xz Mode is more favourable than HD. Before displaying the results, the following points must be noted.

At a given η, r_X and Q_{PX} are calculated as functions of E_{xo}. As E_{xo} is diminished, r_X increases and Q_{PX} decreases. When E_{xo} approaches a lower limit E_G, $r_X \to 1$ and $Q_{PX} \to 0$ showing that E_G is a critical point. For $E_{xo} < E_G$, a solution of (13) yielding the xz Mode threshold does not exist; the xz Mode can exist as a solution only when a sufficiently strong stabilizing $\mathbf{E}_o$ is applied along x. The physical explanation follows along the lines given earlier (§3.1 of [20]). The modification of $\mathbf{E}$ by the director perturbations can bring down the free energy of PD with respect to that of HD if the wavevector of PD takes a sufficiently high value. An expression for E_G results from the method of Oldano *et al.* [11], by expanding the condition (13) in powers of Q_x. The zeroth order term is identically the condition (10). The next term is proportional to Q_x^2. Equating it to zero and solving for E_{xo}, one finds,

$$E_G^2 = \frac{4\pi K_1 \varepsilon_\parallel q^2}{\varepsilon_\perp \varepsilon_A \Delta h^2}; \quad \Delta = \frac{\varepsilon_A(\eta^2 + q^2 - \eta)}{\varepsilon_\parallel(\eta^2 + q^2 + \eta)} \tag{14}$$

where q is a solution of (10). As the perturbations involved have pure modal structure, the method of [28] can also be employed to deduce the critical point (14).

Clearly, E_G is a function of η. Variation of η from a high value shows that E_G increases monotonically with a decrease of η despite a diminution in q as per (10). This means, the range of existence of the xz Mode gets curtailed (equivalently, the range of existence of HD expands) when the anchoring is weakened. For rigid anchoring, $\eta \gg 1$, $q \approx \pi/2$ and $\Delta \approx \varepsilon_A/\varepsilon_\parallel$ so that E_G takes the value E_M given by

$$E_M^2 = \frac{\pi^3 K_1 \varepsilon_\parallel^2}{h^2 \varepsilon_\perp \varepsilon_A^2} \tag{15}$$

which is exactly the expression found for rigid anchoring (see [20], §3.2). E_M is employed to define the dimensionless stabilizing electric field

$$R_E = E_{xo}/E_M.$$

The results for the yz Mode follow exactly as in (13)–(15) except that we replace K_1 by K_2 and employ

$$r_Y = H_{PY}/H_F$$

and Q_{PY} to denote corresponding quantities. The critical point $E_{xo} = E_L$ is given by [see (10) and (14)]

$$E_L^2 = \frac{4\pi K_2 \varepsilon_\parallel q^2}{\varepsilon_\perp \varepsilon_A \Delta h^2}. \tag{16}$$

In the limit of rigid anchoring, E_L reduces to the field E_C (see [20], §3.1). As $E_L < E_G$, the yz Mode always exists over a broader range of E_{xo} values than the xz Mode. Calculation at given η and R_E shows that $r_Y < r_X$ and $Q_{PY} > Q_{PX}$. It is clearly a consequence of K_2 (associated with yz Mode) being less than K_1. Thus, the yz Mode is more favourable than the xz Mode for $E_{xo} > E_L$ when $\mathbf{H}_\perp$ acts along x. When $E_{xo} < E_L$, only HD will form.

For the xyz Mode, ϕ gets coupled elastically to θ despite α being zero and adds to the elastic free energy; but ϕ does not cause modification of $\mathbf{E}$. Hence, the xyz Mode threshold (if it exists) cannot be less than the

threshold of the xz or the yz Mode. The *ansatz* for the perturbations is

$$(\theta, \phi, \psi) = \left(\theta_A \cos\frac{qz}{h}, \phi_A \cos\frac{qz}{h}, \psi_A \sin\frac{qz}{h}\right) \times \sin\left[\frac{Q(C_\mu x + S_\mu y)}{h}\right]$$

so that the wavevector with amplitude Q mades angle μ with the x axis. Substitution in (3)–(5) and use of (7) and (8) yields a compatibility condition from which one obtains $H_\perp$ as a function of Q and μ. This defines a neutral stability surface. If this surface has a minimum $H_{PXY} = H_\perp(Q_{PXY}, \mu_P)$ at $Q = Q_{PXY}$, $\mu = \mu_P$ and if $H_{PXY} < H_F$, we say that the xyz Mode is more favourable than HD.

For the xyz Mode, the derivation of the compatibility condition is complex as it involves the solution of a cubic. It is, however, possible to obtain H_{PXY}, Q_{PXY} and μ_P numerically by the series solution method. Calculations are performed for the parameters of M1 [21] at a reduced temperature of 0·9:

$$(K_1, K_2, K_3) = (16{\cdot}1, 5{\cdot}2, 18{\cdot}3) \times 10^{-7}\,\text{dyne};$$
$$\chi_A = 1{\cdot}39 \times 10^{-7}\,\text{emu};$$
$$\varepsilon_\parallel = 8{\cdot}9; \quad \varepsilon_\perp = 22{\cdot}8; \quad \varepsilon_A = -13{\cdot}9. \quad (17)$$

At $\alpha = 0$, the neutral stability surface shows two minima at $\mu_P = 0$ and $\mu_P = \pi/2$ corresponding to the xz Mode and yz Mode thresholds, respectively; at these μ values, Q_{PXY} coincides, respectively, with Q_{PX} and Q_{PY} calculated for the xz and yz Modes. Hence, the xyz Mode *degenerates* into (either the xz Mode or) the yz Mode when $\mathbf{H}_\perp$ and $\mathbf{E}_0$ are parallel to each other.

The nature of perturbations studied in this work must be clearly understood. As per (7) and (8), the perturbations do not vanish at the substrates. At the yz Mode threshold, for example, we have a solution which yields θ and ψ varying periodically along y with wavevector Q_{PY} even at the substrates. The condition (8) has to be independently imposed for PD due to the finiteness of anchoring energy. For HD, however, (8) is satisfied automatically by (3). Thus, the boundary conditions for HD and PD are different for the present case. In principle, therefore, one can expect changes in the shape of the neutral stability curve as well as in the nature of the transition between HD and PD—especially when anchoring is sufficiently weak. When the anchoring is very strong, θ will nearly vanish at the boundaries; $\psi_{,z}$ will also become correspondingly small at the substrates as per (8) leading to nearly identical boundary conditions for HD and PD. Hence, results for strong anchoring should be qualitatively similar to those obtained earlier [20] for rigid anchoring.

3.2. *Results for PD in M1 at $\alpha \neq 0$*

As with HD (§ 2), PD involves all three perturbations, the presence of ϕ being possible due to the magnetic cross coupling terms a_ϕ and b_θ in the torque equations (4) and (5). The method of solution is similar for all three PD Modes. Consider first the yz Mode. With y dependence of the form $\sin(Q_y y/h)$, (3)–(5) can be reduced to a set of coupled ordinary differential equations. As there are three equations, the method of solution by dependence of perturbations on $\exp(iqz/h)$ (as in § 3.1), leads to a cubic in q with three roots, q_1, q_2, q_3 some of which may be real and the others complex. Each perturbation has to be written as the sum of three terms and (7) and (8) lead to the vanishing of a third order determinant as the compatibility condition. For reasons of convenience, the set of ordinary differential equations are solved numerically by the series solution method which again leads to a similar compatibility condition. We study, in particular, the solution with θ and ϕ symmetric and ψ antisymmetric relative to the sample centre. At a sufficiently elevated R_E and a given magnetic tilt α, r_Y and Q_{PY} can be determined from the minimum of the neutral stability curve. The reduced magnetic threshold and the dimensionless wavevector can be studied as functions of different parameters.

In § 3.1 a true critical point is found between PD and HD when $\mathbf{H}_\perp$ acts along x. Calculation shows that the PD threshold equals the HD threshold and the wavevector of periodicity vanishes in the same limit when the critical point is approached. The question that arises is whether this is true when $\alpha \neq 0$. The answer becomes clear when results are displayed for the different PD Modes. We assume for the moment that the critical point exists and set out to determine it mathematically. The method of [29] is well suited for the purpose. The *ansatz* for yz Mode perturbations with the appropriate dependence on y and z is substituted into (2)–(8). Using (4)–(8), F is calculated upto second order in Q_y such that $F = F_0 + F_1 Q_y^2$. With the HD threshold condition (10), F_0 vanishes identically. Using (9), σ_H is expressed in terms of σ_E at the critical point. The requirement that $F_1 = 0$ leads to the critical condition for the yz Mode:

$$K_1 S_\alpha^2 (q^2 - \sigma_E)^2 + q^2 C_\alpha^2 (K_2 q^2 - K_3 \Delta\sigma_E) = 0 \quad (18)$$

where q satisfies (10) and Δ is defined in (14). When $\alpha = 0$, (18) reduces to (16) an we have only one critical point. For general (nonzero) values of α, (18) yields two critical values for σ_E:

$$\frac{\sigma_E}{q^2} = \frac{e(\alpha) \pm (e^2(\alpha) - j(\alpha)\gamma_1 S_\alpha^2)^{1/2}}{\gamma_1 S_\alpha^2}; \quad \beta_2 = \frac{K_2}{K_3};$$
$$j(\alpha) = \beta_2 C_\alpha^2 + \gamma_1 S_\alpha^2; \quad e(\alpha) = \gamma_1 S_\alpha^2 + \frac{\Delta C_\alpha^2}{2}. \quad (19)$$

The critical fields denoted by E_{Y1} and E_{Y2} (with $E_{Y1} > E_{Y2}$) determine the range of existence of the yz Mode to be $E_{Y1} < E_{xo} < E_{Y2}$. When the quantity under the root sign is positive, the roots are both real and unequal. The roots become equal when $\alpha = \alpha_Y$ corresponding to $\sigma_E = \sigma_Y$ such that

$$\tan^2 \alpha_Y = \frac{K_3^2 \Delta^2}{4K_1(K_2 - K_3\Delta)}; \quad \sigma_Y = \frac{q^2(2K_2 - K_3\Delta)}{K_3\Delta}. \tag{20}$$

Obviously, the yz Mode cannot exist for $\alpha > \alpha_Y$. Equations (18)–(20) reduce to their counterparts for rigid anchoring in the limit $\Delta \to \varepsilon_A/\varepsilon_\perp$.

Results for the xz Mode can be obtained by interchanging K_1 and K_2 (equivalently, β_2 and γ_1) in the expressions and equations for the yz Mode. The critical equation for the xz Mode becomes

$$K_2 S_\alpha^2 (q^2 - \sigma_E)^2 + q^2 C_\alpha^2 (K_1 q^2 - K_3 \Delta \sigma_E) = 0 \tag{21}$$

yielding the critical fields E_{X1} and E_{X2} determined from

$$\frac{\sigma_E}{q^2} = \frac{g(\alpha) \pm (g^2(\alpha) - f(\alpha)\beta_2 S_\alpha^2)^{1/2}}{\beta_2 S_\alpha^2};$$

$$f(\alpha) = \gamma_1 C_\alpha^2 + \beta_2 S_\alpha^2; \quad g(\alpha) = \beta_2 S_\alpha^2 + \frac{\Delta C_\alpha^2}{2}. \tag{22}$$

The limit of existence of the xz Mode at which E_{X1} and E_{X2} coincide is found to be $\alpha = \alpha_X$ occurring at $\sigma_E = \sigma_X$ with

$$\tan^2 \alpha_X = \frac{K_3^2 \Delta^2}{4K_2(K_1 - K_3\Delta)}; \quad \sigma_X = \frac{q^2(2K_1 - K_3\Delta)}{K_3\Delta}. \tag{23}$$

For M1 parameters (17), $\alpha_X > \alpha_Y$; the α range of existence of the xz Mode is wider than that of the yz Mode. Obviously, the two will coincide when the splay and twist elastic constants are equal.

α_Y and α_X are functions of the anchoring strength. The critical fields for the two PD Modes are found from (19) and (22) after q is calculated from (10) for a given η. Suppose $h = 250\,\mu m$. With $B = 10^{-2}\,erg\,cm^2$, $\eta = 136$. This corresponds to *strong anchoring*. Decrease of B by two orders of magnitude makes $\eta = 1{\cdot}36$ for the same sample thickness; this can be regarded as *weak anchoring*. Calculations are presented for one other η value (see figure 1 (*c*)) for clarification of some results, but this value is unrealistically small. The critical fields obtained from (19) and (22) are scaled by E_M and plotted in figures 1 (*a*), 1 (*b*) for two η values. The presence of the curves 1′ and 2′ as well as a part of curve 1 being represented by a dashed line will both be explained in due course. For the present, the following points may be noted with special reference to figure 1 (*a*). (i) The region of existence of the yz Mode (YZ) is almost completely surrounded by that of the xz Mode (XZ) except for weak enough $\mathbf{E}_o$ where only the yz Mode survives. (ii) At fixed E_{xo}, a given PD Mode is extinguished when α exceeds a limiting value which can be read off from the intersection of a suitably drawn horizontal line with the corresponding phase boundary. The α limits for the xz and yz Modes can be computed by solving (21) and (18), respectively, at the given σ_E. (iii) The yz Mode exists in the low α range and the xz Mode in the higher α range [consequence of (i)]. (iv) When α is high enough ($\mathbf{H}_\perp$ is applied sufficiently away from $\mathbf{E}_o$), only HD exists regardless of the strength of the stabilizing $\mathbf{E}_o$. HD alone survives for weak enough $\mathbf{E}_o$ also. (v) In the overlap region (marked with XZ and YZ), both PD Modes exist as solutions. The PD Mode with lower threshold is taken to be the more favourable Mode by actual

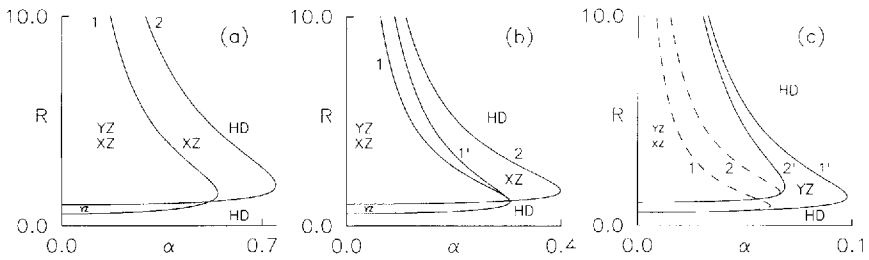

Figure 1. Initial uniform orientation of the nematic director along z. The sample planes are at $z = \pm h$. Material parameters are those of M1 (17) so that $\mathbf{H}_\perp$ destabilizes the orientation while $\mathbf{E}_o$ (applied along x) stabilizes it; α is the tilt of $\mathbf{H}_\perp$ away from $\mathbf{E}_o$ in the xy plane. The yz and xz Modes are periodic deformations with periodicity along y and x, respectively. Plots of R_X (curves 2 and 2′) and R_Y (curves 1 and 1′) versus α (radian). Curves 1 and 1′ correspond to a second order and a first order transition, respectively, between HD and the yz Mode, Curves 2 and 2′ are similarly defined for the xz Mode. R_X is the ratio of the critical field for the xz Mode and E_M (15). R_Y is the critical field for the yz Mode scaled by E_M. Curves 1, 2 result from (19), (22), respectively; the primed curves are obtained numerically. The regions XZ, YZ and HD correspond to, respectively, the xz Mode, the yz Mode and the aperiodic or homogeneous deformation. The dashed portion of a curve is of no physical significance. $\eta = Bh/K_3$ where B is the anchoring strength at the boundaries and K_3 the bend elastic constant. The diagrams are drawn for $\eta =$ (*a*) 136, (*b*) 1·36 and (*c*) 0·136 (see § 3·2).

computation (see figures 2–5). (vi) The α ranges of existence of both PD Modes shrink when η is diminished (compare figures 1(*a*) and 1(*b*)). (vii) Each diagram is valid for a particular value of η which, in turn, depends on the product Bh. Hence, figure 1(*b*) is equally valid for $B = 10^{-2}$ erg cm^{-2} if the sample thickness is reduced by a factor of hundred. This scaling holds for other results too. (vii) For a given η, the critical curves for the xz and yz Modes intersect at $\alpha = \alpha_B$ and $E_{xo} = E_B$. From (19), (22), (14) and (16),

$$\sin^2 \alpha_B = \frac{\Delta^2}{\Delta^2 + (\beta_2 + \gamma_1 - \Delta)^2}; \quad E_B^2 = E_G^2 + E_L^2. \quad (24)$$

Figures 2–5 contain plots of PD thresholds and wavevectors as functions of different parameters. Results are presented for only the xz and yz Modes. When α is not zero, the xyz Mode threshold can be calculated as described in § 3.1. The neutral stability surface shows a minimum $H_\perp = H_{PXY}$ at a nontrivial value of μ_P which varies with both R_E and α. For the parameters (17), the xyz Mode threshold is higher than the thresholds of the other PD Modes; hence, results are not presented for the xyz Mode. The variation of the xyz Mode threshold and related parameters is analogous to that found for rigid anchoring (see figures 2 and 3 of [20]).

The results of figures 2 and 3 for strong anchoring are in accord with figure 1(*a*) and are also similar to those of [20]. When α is close to zero (see figures 2(*a*) and 2(*b*)), the second critical point is extremely high, hence the behaviour of r and Q_P is similar to that for $\alpha = 0$. With increase of R_E from the lower critical point, r diminishes from 1 and Q_P increases from zero. The xz Mode threshold is higher than that of the yz Mode, hence only the yz Mode is of real interest. This means, the stripes will have periodicity along y for all R_E.

The character of variations of r and Q_P changes drastically when α is higher (see figures 2(*c*) and 2(*d*)). The presence of two cut offs for both PD Modes is evident and these can be read off from figure 1(*a*) by drawing a vertical line at the requisite α value and noting the intersections with the respective phase boundaries. While the yz Mode is more favourable for weak $\mathbf{E}_o$, the xz Mode should be observable for stronger stabilizing fields. Should this crossover occur, it will manifest through a discontinuous change in the stripe width as well as direction of periodicity. For high enough R_E when even the xz Mode has been quenched, only HD will exist.

The dependence of r and Q_P on α at a fixed strength of the stabilizing $\mathbf{E}_o$ is again in accord with figure 1(*a*). A given PD Mode gets quenched when α exceeds the limit which is got from figure 1(*a*) by noting the intersection of a horizontal line drawn at the requisite R_E value. At a given σ_E, the limits α_G and α_L for the xz and yz Modes are obtained by solving (21) and (18), respectively:

$$\cos^2 \alpha_G = \frac{K_2(q^2 - \sigma_E)^2}{K_2(q^2 - \sigma_E)^2 - K_1 q^4 + K_3 \Delta\sigma_E q^2};$$

$$\cos^2 \alpha_L = \frac{K_1(q^2 - \sigma_E)^2}{K_1(q^2 - \sigma_E)^2 - K_2 q^4 + K_3 \Delta\sigma_E q^2}. \quad (25)$$

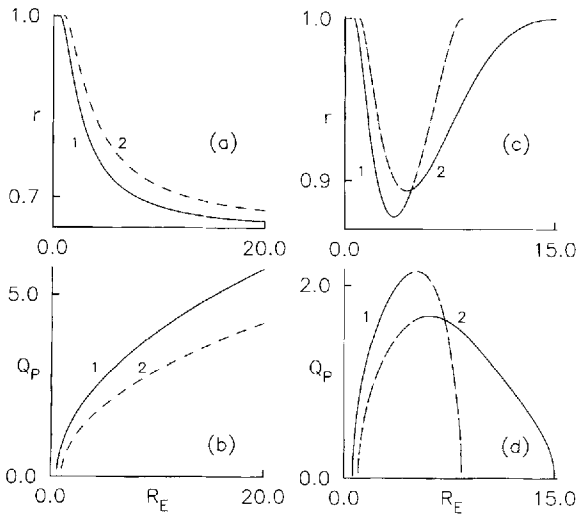

Figure 2. Plots of reduced thresholds of the xz and yz Modes (r_X, r_Y) and the respective dimensionless wavevectors (Q_{PX}, Q_{PY}) as functions of R_E for two values of the magnetic tilt α (see caption of figure 1 for details). Strong anchoring with $\eta = 136$. Curves 1 and 2 represent the yz and the xz Modes, respectively. $\alpha = (a, b)$ 0·01, (c, d) 0·2 radian. The results are in agreement with figure 1(*a*) (see § 3.2).

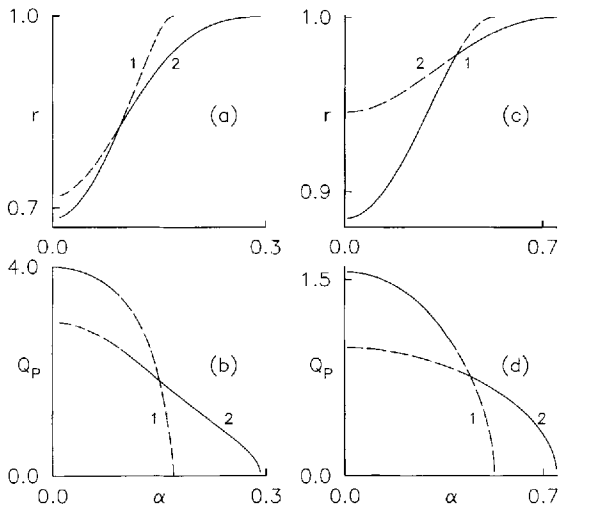

Figure 3. Variation of dimensionless magnetic thresholds and wavevectors for xz (curves 2) and yz (curves 1) Modes with the magnetic tilt angle. Strong director anchoring with $\eta = 136$. $R_E = (a, b)$ 10, (c, d) 2. Both PD Modes get extinguished when α is sufficiently high. The critical points can be read off from figure 1(*a*) (see § 3.2).

Interestingly, α_G at $R_E = 10$ is less than its value at $R_E = 2$ (see figures 1 (*a*) and 3). The *yz* Mode is found to exist for low α ($\mathbf{H}_\perp$ close to the *x* axis) while the *xz* Mode dominates in the higher α range. When α is sufficiently high even the *xz* Mode gets quenched and only HD should be possible. The crossover should again be heralded by a discontinuous change in the wavevector. Some of these results can be interpreted as explained earlier (see § 3.1 and 3.4 of [20]).

Figures 4 and 5 depict results for the weak anchoring case. The variation of r and Q_P with R_E for $\alpha = 0{\cdot}01$ has not been included. The curves are very similar in shape to those of figures 2 (*a*) and 2 (*b*). Figure 4 is drawn for two α values, both of them somewhat high. The variations of r_X and Q_{PX} are qualitatively similar to those found in figures 2 and 3; however, the *yz* Mode threshold and wavevector exhibit a somewhat different dependence. The reason for this becomes clear by studying the neutral stability curve for the *yz* Mode when anchoring is weak and a reasonably strong $\mathbf{E}_o$ is imposed; say, $E_{xo} = E_1$.

Then, the compatibility condition for the *yz* Mode yields $\mathbf{H}_\perp(Q_y)$ as a function of Q_y. When α is close to zero (say, 0·001 radian), $H_\perp$ diminishes continuously with increase of Q_y and the true minimum at $Q_y = Q_{PY}$ is the *yz* Mode threshold. When α is higher (say, 0·1 radian), the shape of the neutral stability curve remains unchanged as long as the stabilizing $\mathbf{E}_o$ is not very strong (typically, $\sigma_E < \sigma_Y$ of equation (20)). This means, decrease of E_{xo} from E_1 leads to the critical point E_{Y2} on the lower branch of the curve 1 in figure 1 (*b*) (see * in figure 4 (*a*)). With Q_{PY} as the order parameter, the transition from *yz* Mode to HD is one of second order. When E_1 is such that $\sigma_E > \sigma_Y$, the shape of the neutral stability curve changes. Increase of Q_y from zero leads first to a weak maximum $H_1 = H_\perp(Q_1)$ at $Q_y = Q_1$, say; $H_1 > H_F$. Further increase of Q_y leads to decrease in $H_\perp(Q_y)$ and a true minimum H_{PY} at some Q_{PY} where $H_\perp(Q_{PY}) < H_F$; this is the true *yz* Mode threshold. In figures 4 (*a*) and 4 (*b*), both extremes have been plotted with curves 1 corresponding to the minimum and curves 1′ representing the maximum. When E_{xo} is increased above E_1, H_1 and Q_1 diminish; when E_{xo} approaches the upper critical value E_{Y1} (see #, figure 4 (*a*)), $H_1 \to H_F$ and $Q_1 \to 0$. But H_{PY} and Q_{PY} exist beyond $E_{xo} = E_{Y1}$ with H_{PY} equalling H_F at some $E_{xo} > E_{Y1}$; but here, H_{PY} is not zero (see figure 4 (*b*)); see ** in figure 4 (*a*)). This is the true upper cut-off point for the *yz* Mode as beyond this point, $H_{PY} > H_F$. This transition from the *yz* Mode to HD is, therefore, one of first order. Beyond the true cut-off, the *yz* Mode exists as a solution over a range of E_{xo} but is of only academic interest. The behaviour at $\alpha = 0{\cdot}2$ radian is similar (see figures 4 (*c*) and 4 (*d*)).

Interestingly, the behaviour of the *xz* Mode threshold and wavevector is similar to that found in figure 2 even

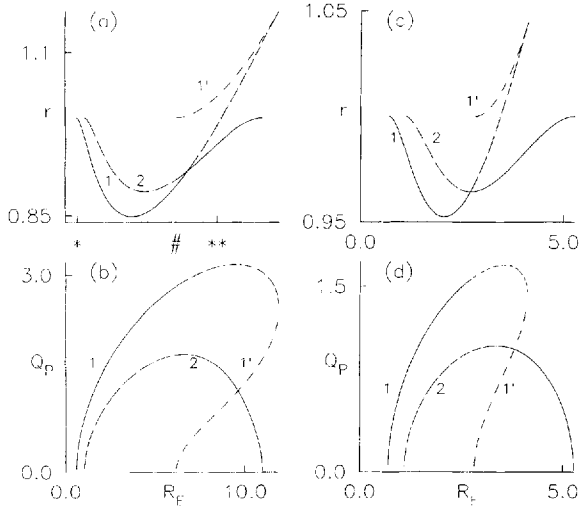

Figure 4. Case of weak anchoring with $\eta = 1{\cdot}36$. Details as in figure 2 with $\alpha = (a, b)$ 0·1, (c, d) 0·2 radian. In figure 4 (*a*), the R_E axis is not labelled with numbers for convenience. Curves 1 and 2 represent plots of true minima of the neutral stability curves for the *yz* and *xz* Modes, respectively. Curve 1′ is the locus of a weak maximum in the neutral stability curve for the *yz* Mode and meets the R_E axis (see figure 4 (*b*)) at a pseudo critical point (#). For stronger electric strengths, the *yz* Mode threshold and wavevector are both double valued functions. The true upper cut off field for the *yz* Mode (where the *yz* Mode and HD have equal magnetic threshold) is represented by ** and can be read off from curve 1′ of figure 1 (*b*) (see § 3.2).

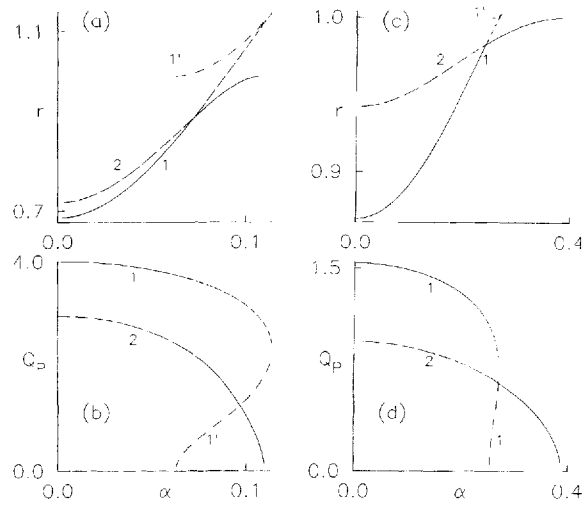

Figure 5. Weak anchoring with $\eta = 1{\cdot}36$. Details as in figure 3 for plots of thresholds and wavevectors versus the magnetic tilt angle α. $R_E = (a, b)$ 10, (c, d) 2. Compare with figure 1 (*b*). Curves 1, 1′ and 2 have the same significance as in figure 4. The transition from the *yz* Mode to HD with increase of α is discontinuous (see § 3.2).

at $\eta = 1{\cdot}36$. The general effect of decrease in η on either PD Mode is a diminution of wavevector and enhancement of threshold relative to H_F. Due to the reasons mentioned in the previous paragraph, the upper cut off for the yz Mode has to be determined numerically. This is represented by curve 1′ in figure 1 (*b*). It is seen that curves 1 (corresponding to E_{Y1}) and 1′ coalesce when σ_E decreases to σ_Y. Similar departure is found in the behaviour of the yz Mode for α variation with weak anchoring (see figure 5).

When the anchoring is weak neither θ nor $\psi_{,z}$ vanishes at the boundaries. For PD, $\psi_{,z}$ has the same periodic modulation as θ. As $\varepsilon_A < 0$, the perturbation $\psi_{,z}$ actually has a destabilizing effect. With this destabilizing influence varying in phase with θ, one can expect departures in the behaviour of both the PD Modes with respect to the strong anchoring limit. Both Modes obey boundary conditions that differ from those imposed on HD. In both cases, explicit limits are not imposed on electric field perturbations along sample peripheries. It is, therefore, surprising that the xz Mode is not affected at $\eta = 1{\cdot}36$. This doubt is removed by looking at figure 1 (*c*) drawn for a very small value of B; even the xz Mode undergoes a first order transition at its upper cut-off (curves 2′ in figure 1 (*c*) represent the true cut-off for the xz Mode); again, curves 2 and 2′ coalesce near $\sigma_E = \sigma_X$ of (23). Detailed calculations are not presented for this unrealistic value of η. But interestingly, the region of existence of the xz Mode is now surrounded by that of the yz Mode.

4. Material with $\varepsilon_A > 0$, $\chi_A < 0$

In such a material, $\mathbf{H}_\perp$ becomes a stabilizing field while $\mathbf{E}_0$ tends to destabilize the initial orientation. CCH-7 is a typical material having the following parameters at a reduced temperature of 0·932 [22]:

$$(K_1, K_2, K_3) = (7{\cdot}25, 3{\cdot}48, 11{\cdot}46) \times 10^{-7}\,\text{dyne};$$
$$\chi_A = -3{\cdot}22 \times 10^{-8}\,\text{emu};$$
$$\varepsilon_\parallel = 8{\cdot}01; \quad \varepsilon_\perp = 3{\cdot}72; \quad \varepsilon_A = +4{\cdot}29. \quad (26)$$

The effect of $\mathbf{H}_\perp$ applied along symmetry directions (x and y) is first studied.

4.1. *Results for PD at $\alpha = 0$ and $\alpha = \pi/2$*

Let α be zero. Solutions can be sought for all three PD Modes. For the xz and yz Modes, ϕ gets decoupled and damps out. The threshold condition (13) is still valid for the xz Mode except that now we determine $E_{xo}(Q_x)$ as a function of Q_x. When $H_\perp$ is high enough, E_{xo} is close to E_F of (12) when Q_x is small. Increase of Q_x leads to a diminution in E_{xo} and a minimum at $E_{PX} = E_{xo}(Q_{PX})$ at some $Q_x = Q_{PX}$ which is the xz Mode threshold. The xz Mode exists as a solution if $H_\perp > H_G$; for $H_\perp < H_G$, only HD prevails. For rigid anchoring, $H_G \to H_C$ (see equation (27) of [20]). The definitions are as follows [see also (10)]:

$$H_G^2 = \frac{K_3 q^2}{\chi_A h^2}\left(1 - \frac{K_1}{K_3 \Delta}\right);$$
$$H_C^2 = -\frac{K_3 \varepsilon_\parallel \pi^2}{4\chi_A \varepsilon_A h^2}\left(\frac{K_1}{K_3} - \frac{\varepsilon_A}{\varepsilon_\parallel}\right). \quad (27)$$

H_C can be used to measure $H_\perp$ in terms of the reduced field $R_H = H_\perp / H_C$ while the xz Mode electric threshold can be represented by $r_X = E_{PX}/E_F$. With decrease of η, the ratio H_G/H_F increases; i.e., the domain of existence of HD expands relative to that of the xz Mode with weakening of the director anchoring.

The yz Mode is treated similarly with K_2 replacing K_1. The critical condition for the existence of the yz Mode is that $H_\perp > H_L$ with

$$H_L^2 = \frac{K_3 q^2}{\chi_A h^2}\left(1 - \frac{K_2}{K_3 \Delta}\right). \quad (28)$$

It is known [20] that H_L is not real for the parameters (26) when anchoring is rigid. Thus, the yz Mode can exist as a solution even at $H_\perp = 0$ with a threshold *lower* than that of HD. As $K_2 < K_1$, the yz Mode threshold is found to be lower than the xz Mode threshold even for strong $\mathbf{H}_\perp$. Hence, the xz Mode is of only academic importance when $\mathbf{H}_\perp$ acts along x. A similar conclusion follows for strong anchoring. But H_L^2 becomes positive when the anchoring is weakened sufficiently; then a critical point exists between the yz Mode and HD; still, this point is lower than H_G. From (28) and (10), this cut-off value η_C of η is deduced as the solution of

$$K_3 \Delta = K_2; \quad (29)$$

the yz Mode has a critical point if $\eta < \eta_C$. For the parameters (26), $\eta_C = 3{\cdot}158$.

The yz Mode threshold $E_{PY} = E_{xo}(Q_{PY})$ occurs at the minimum $Q_y = Q_{PY}$ of the neutral stability curve. We employ the dimensionless quantity $r_Y = E_{PY}/E_F$ to measure the yz Mode threshold. The xyz Mode is again of no interest as it degenerates into either the xz Mode (wavevector along x) or the yz Mode (wavevector along y). The yz Mode, therefore, remains the physically real PD Mode at $\alpha = 0$. Figure 6 represents these conclusions.

The case of $\mathbf{H}_\perp$ acting along $\alpha = \pi/2$ can be treated as before with ϕ damping out and leaving θ, ψ. As a_θ vanishes in (4), the θ–ψ pair obeys the equations corresponding to $H_\perp = 0$. The xz Mode cannot exist in the absence of $\mathbf{H}_\perp$. Hence, the yz Mode will prevail as long as the anchoring is not very weak. If $\eta < \eta_C$, HD will occur involving θ and ψ.

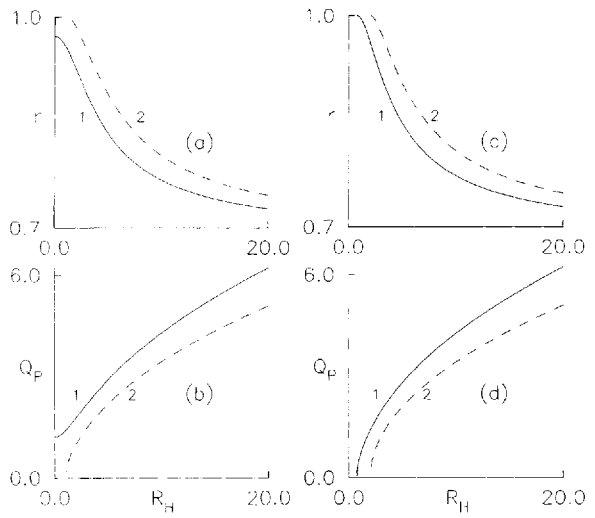

Figure 6. Initial uniform homeotropic alignment along z between plates $z = \pm h$. The material is CCH-7 (26) with $\chi_A < 0$ and $\varepsilon_A > 0$ so that $\mathbf{E}_0$ along x destabilizes the orientation and $\mathbf{H}_1$ in the xy plane stabilizes it. Particular case of $\mathbf{H}_\perp$ acting along x axis (magnetic tilt angle $\alpha = 0$). The xyz Mode degenerates into either the xz Mode (curves 1) or the yz Mode (curves 2). Plots of the reduced electric thresholds r_X, r_Y and the dimensionless wavevectors Q_{PX}, Q_{PY} as functions of the reduced stabilizing magnetic field, R_H for strong anchoring (a, b) $\eta = 218$ and weak anchoring (c, d) $\eta = 2{\cdot}18$. A dashed curve represents results of no physical interest (see §4.1).

The results of this section are valid for a material such as 5CB [20] which has positive anisotropies provided that a stabilizing $H_\parallel$ is assumed to act along z (obviously, with $H_\perp = 0$). The definitions for the critical fields in (27) and (28) hold with a negative sign in front of χ_A. With these changes, figure 6 is identically valid for a hypothetical material having the same parameters as CCH-7 (26) but with χ_A positive. We again assume that $H_\parallel = 0$.

4.2. *Results for PD at general values of* α

Computation of thresholds for (26) shows that the xz and yz Modes have higher thresholds than the xyz Mode when α takes general values. Hence, only the xyz Mode is studied in this section. For (26), the neutral stability surface of the xyz Mode shows a minimum at $E_{PXY} = E_{xo}(Q_P, \mu_P)$ corresponding to the reduced threshold

$$r_{XY} = E_{PXY}/E_F.$$

For zero magnetic field as well as for $\mathbf{H}_\perp$ impressed along symmetry directions ($\alpha = 0, \pi/2, \pi$), the xyz Mode degenerates into the yz Mode (i.e., $\mu_P \to \pi/2$).

Assuming a critical point for the transition between the xyz Mode and HD, this should occur in the limit $Q_{PXY} \to 0$ and $E_{PXY} \to E_F$. In this limit, μ and α assume values μ_C and α_C, respectively. Using the method of [28], the critical condition becomes [see (10), (19) and (22) for definitions]

$$\sigma_H^2 S_\alpha^2 \left[S_\alpha^2 f(\mu) + C_\alpha^2 j(\mu) - \Delta - S_\alpha C_\alpha \frac{dj(\mu)}{d\mu} \right] + \sigma_H q^2 \left[\Delta + \Delta S_\alpha^2 + S_\alpha C_\alpha \frac{dj(\mu)}{d\mu} - 2S_\alpha^2 f(\mu) \right] + q^4 [f(\mu) - \Delta] = 0 \quad (30)$$

and this relates σ_H, α and μ. For a given magnetic tilt α, (30) can be used to find the critical value of $H_\perp$. When R_H is fixed, (30) determines the α range of existence of the xyz Mode. For the moment, σ_H is assumed fixed. Solving for μ, we can express S_μ as a function of σ_H and α. Real solutions cease to exist when $\alpha > \alpha_C$ with

$$\sin^2 \alpha_C = \frac{q^2[K_3\Delta(q^2 - \sigma_H) - K_2 q^2]}{\sigma_H[\sigma_H(K_2 - K_3\Delta) + q^2(K_3\Delta - 2K_2)]},$$

$$\sin^2 \mu_C = \frac{(\sigma_H \sin^2 \alpha_C - q^2)^2}{(\sigma_H \sin^2 \alpha_C - q^2)^2 + (\sigma_H \sin \alpha_C \cos \alpha_C)^2}. \quad (31)$$

At given σ_H and η, q is found from (10); then α_C and μ_C can be calculated if they exist. The limiting value for α_C is $\pi/2$. Then, $\sin \alpha_C$ is unity; clearly, then μ_C is $\pi/2$ (the xyz Mode degenerates into the yz Mode). From (31), this leads directly to the definition of η_C (29). Thus, the xyz Mode (as well as the yz Mode) will have a critical point only if $\eta < \eta_C$. For $\eta > \eta_C$, these Modes will exist as solutions over the entire α range regardless of the $\mathbf{H}_\perp$ imposed. As stated earlier, the yz Mode threshold is higher than the xyz Mode threshold for general α.

Figure 7 displays the xyz Mode threshold and wavevector as functions of the magnetic tilt angle α for two different R_H. Figures 7(*a*)–(*c*) correspond to strong anchoring and the results are similar to those obtained for rigid anchoring (see figures 4(*d*)–(*f*) of [20]). The xyz Mode exists over the entire α range and turns into the yz Mode when $\mathbf{H}_\perp$ acts along the symmetry directions. When α is small, the stripes should become sharper with increase of R_H. The curves for threshold and wavevector amplitude are symmetric about $\alpha = \pi/2$. The shape of the μ_P curve results from the need to preserve the value of the term $S_\alpha C_\alpha S_\mu C_\mu$ under a reflection in the $\alpha = \pi/2$ line.

Figures 7(*d*)–(*f*) are drawn for weak anchoring with $\eta < \eta_C$. The xyz Mode now has a critical point with HD. For the given R_H, the (α_C, μ_C) coordinates of the critical point are well represented by (31). Interestingly, α_C increases when the stabilizing $\mathbf{H}_\perp$ becomes weaker. Hence, the shape of the phase diagram for the xyz Mode should be similar to the curves of figure 1.

Figure 8 summarizes the companion calculations for the variation of the stabilizing magnetic strength.

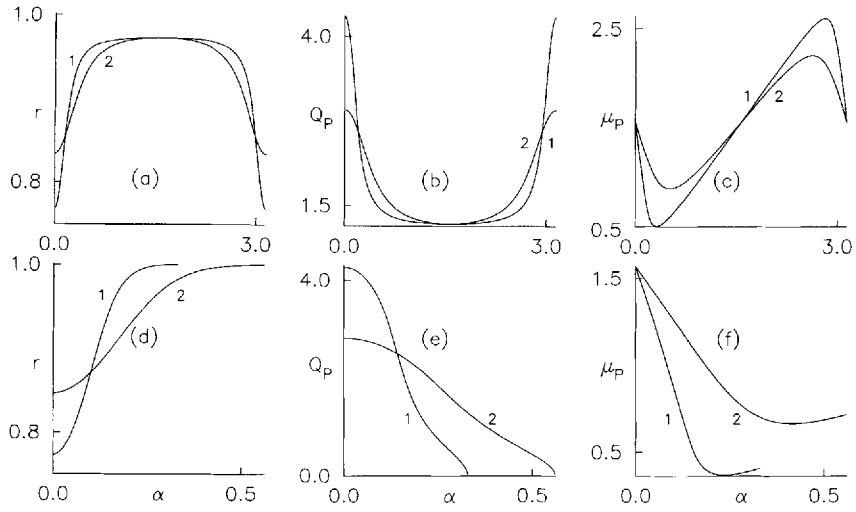

Figure 7. Details as in figure 6. Variations of the reduced *xyz* Mode threshold (r_{XY}), dimensionless wavevector (Q_{PXY}) and tilt of the wavevector with *x* axis (μ_P) with magnetic tilt angle α; the parameters (26) are those of CCH-7. The *xz* and *yz* Mode thresholds are not shown as they are higher than the *xyz* Mode threshold. $\eta = (a, b, c)$ 218 (strong anchoring); (d, e, f) 2·18 (weak anchoring with $\eta < \eta_C$ of equation (29)). Curves are drawn for $R_H = (1)$ 10, (2) 5. For a given R_H, the *xyz* Mode ceases to exist when $\alpha > \alpha_C$ (31) provided that the anchoring is weak enough; only HD will remain in the higher α range. The parameters of the critical point are in agreement with (31) (see §4.2).

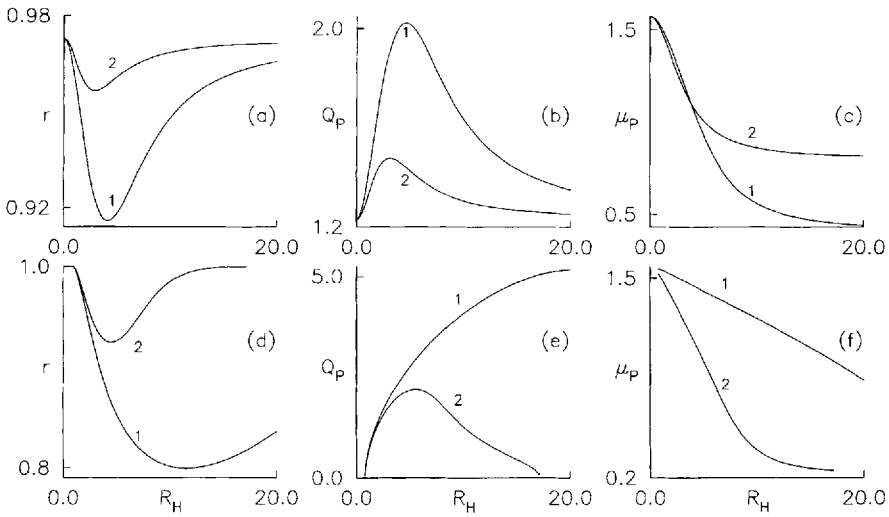

Figure 8. Details as in figures 6 and 7. Plots of r_{XY}, Q_{PXY} and μ_P as functions of R_H, the reduced stabilizing magnetic strength. $\eta = (a, b, c)$ 218 (strong anchoring); $\eta = (d, e, f)$ 2·18 (weak anchoring). In (a, b, c), the magnetic tilt angle $\alpha = (1)$ 0·4, (2) 0·8 radian. In (d, e, f), $\alpha = (1)$ 0·05, (2) 0·2 radian. As $\eta < \eta_C$ of (29) in (d, e, f), *the xyz* Mode has critical points with HD. The parameters of the critical points can be calculated from (31) (§4.2).

Diagrams have not been presented for low α where the variations of r_{XY} and Q_{PXY} are found to be similar to those for the *yz* Mode in figure 6. Results for strong anchoring (figures 8(*a*)–(*c*)) closely resemble those obtained for rigid anchoring (see figures 4(*a*)–(*c*) of [20]). The *xyz* Mode exists for all values of R_H. When R_H is high, $\mu_P \to \alpha$; i.e., the direction of the wavevector approaches that of $\mathbf{H}_\perp$ in the *xy* plane. No critical point exists between *xyz* Mode and HD. For weak anchoring, the η chosen is less than η_C of (29). Critical points now exist between the *xyz* Mode and HD (see figures 8(*d*)–(*f*)). At $\alpha = 0{\cdot}05$ only the lower point is in evidence; both points are seen when α is higher. The critical values R_C of R_H at a given α can be calculated from (31) by solving for σ_H in terms of α; clearly, μ_C is given by (31) with α being written for α_C. The critical points so calculated agree well with those found in figure 8. While the upper critical point varies considerably with α, the lower one does not seem to change much. This again indicates the possible shape of the phase diagram.

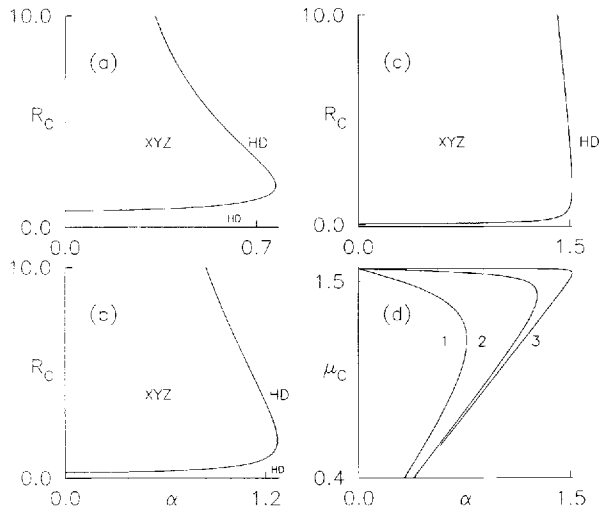

Figure 9. Phase diagrams for the *xyz* Mode in the R_C–α plane. At a given magnetic tilt angle α, R_C is the scaled critical field between the *xyz* Mode and HD. Plot of R_C versus α gives the phase boundary separating the *xyz* Mode and HD. Also plotted is μ_C the tilt angle of the *xyz* Mode wavevector with *x* axis at the critical point. R_C and μ_C can be calculated from (31). $\eta = (a)$ 2·18, (*b*) 3·01, (*c*) 3·15. In (*d*), μ_C is plotted for $\eta = (1)$ 2·18, (2) 3·01, (3) 3·15. It should be remembered that parts of the μ_C curves are drawn for low values of α which are not represented in figures 9(*a*)–(*c*) (§4.2).

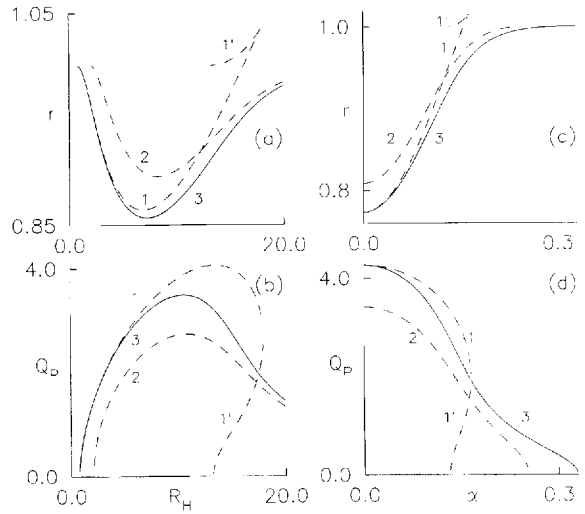

Figure 10. Illustration of the variation of the thresholds and wavevectors for the *yz* Mode (curves 1, 1'), the *xz* Mode (curves 2) and the *xyz* Mode (curves 3). Curves 1' indicate regions where the *yz* Mode threshold and wavevector are double valued. Compare figures 10(*a*) and 10(*b*) with figure 4, and figures 10(*c*) and 10(*d*) with figure 5. Weak anchoring with $\eta = 2{\cdot}18$. In (*a*, *b*), $\alpha = 0{\cdot}1$ radian. In (*c*, *d*), $R_H = 10$. When the anchoring is sufficiently weak, the transition between HD and the *yz* Mode can become discontinuous (see §4.2).

The phase diagrams for the *xyz* Mode are shown in figure 9(*a*)–(*c*) for different η values lower than η_C (29). The close resemblance with figure 1 is evident. With (31), the corresponding values of μ_C are also calculated (see figure 9(*d*)). The α range of the *xyz* Mode expands when η increases towards η_C (see figures 9(*a*)–(*c*)). Variation of α at a given R_H value yields one critical point; variation of R_H at a fixed α may yield two critical points if α is sufficiently high.

When the anchoring is weak, the *yz* Mode behaves (see figure 10) in a way similar to that found in §3.2 for a different class of PD. The curves for the *xz* and *yz* Mode are shown with dashed lines as both Modes are unfavourable compared to the *xyz* Mode. The transition between the *xz* Mode and HD is one of second order; this is also true for the *xyz* Mode. In the low R_H region, the *yz* Mode has a true critical point with HD (see figures 10(*a*) and 10(*b*)). The transition from the *yz* Mode to HD in the higher R_H range becomes one of first order. The transition between the *yz* Mode and HD with α variation (see figures 10(*c*) and 10(*d*)) is also found to be of a similar nature.

5. Conclusions and limitations of the mathematical model

The mathematical model of [20] developed for rigid anchoring has been extended to the case of weak anchoring of the Rapini–Papoular type with both surfaces having identical anchoring strengths. The occurrence of PD under the action of crossed **E** and **H** fields has been studied with both fields applied in the plane of the sample. Results can be presented in scaled form through suitably defined reduced fields and wavevectors using the dimensionless parameter η of (10) to measure the anchoring strength. For a given anchoring strength at the surfaces (i.e., for a given surface treatment), results for weak anchoring can be simulated in thinner samples. The materials chosen [M1 (17) and CCH-7 (26)] have anisotropies of opposite sign. When η is high enough, all conclusions are qualitatively identical to those of [20].

In M1, PD is caused by the destabilizing action of $\mathbf{H}_\perp$ provided a stabilizing $\mathbf{E}_o$ of suitable strength is present. The direction and amplitude of the periodicity wavevector change discontinuously when the tilt of $\mathbf{H}_\perp$ with $\mathbf{E}_o$ is changed in the sample plane. PD is completely suppressed in favour of HD when the magnetic tilt increases beyond a certain limit; the situation is similar when the applied stabilizing $\mathbf{H}_\perp$ is either too strong or too weak. Thus, there exists at least one critical point between PD and HD with the transition between PD and HD at the critical point being one of second order. In CCH-7, on the other hand, the $\mathbf{E}_o$ induced PD can exist even in the absence of a stabilizing $\mathbf{H}_\perp$; the

wavevector amplitude and orientation change continuously with magnetic tilt. There is no critical point between PD and HD. Tentative explanations for these results have been given in [20] in the rigid anchoring limit.

Reduction of η by two orders causes the range of existence of PD to shrink in both materials; this deleterious effect is similar to that predicted for other classes of PD [11]. When $H_\perp$ is varied at sufficiently high magnetic tilt, the transition between PD and HD at the higher field limit is found to be one of first order in M1. A possible reason for this is the enhanced difference between the boundary conditions for PD and HD caused by weak anchoring; the PD threshold cannot remain single valued when the upper critical point is approached. Phase diagrams contrast the predicted and true phase boundaries between PD and HD. The effect on PD in CCH-7 is similar. If η is less than a certain value η_C, a critical point exists between the *xyz* Mode and HD; the direction of the wavevector can take non-trivial values at the transition point.

With the assumption of equal anchoring strengths at the boundaries, perturbations with definite spatial symmetry can be studied. The independent solution with higher threshold and opposite spatial symmetry can be left uninvestigated. If the sample walls have different anchoring strengths, the boundary conditions at the two surfaces will be such that the governing equations will not support solutions with pure symmetry. Each perturbation will be the sum of two parts—one odd and the other even relative to $z = 0$ so far as z variation is concerned. This mixing up should lead to an increase in the PD threshold relative to the HD threshold and a curtailment of the range of existence of PD. In the case of CCH-7, for instance, a critical point between the *xyz* Mode and HD may emerge if one sample plane has sufficiently weak anchoring even when the director is strongly anchored at the other plane.

Linear perturbation calculations are valid only upto the threshold. Possible effects occurring beyond threshold have to be separately investigated. As noted already, all boundary conditions on the electric field are not imposed. Surface elastic constants are not included; hence, the results may hold only for sufficiently thick samples. The nematic is assumed to be an insulator with no free charges (ionic impurities). This is generally not true of commercially available material. The possibility of EHD convection [23] occurring in the place of the static periodic distortion has to be studied with the full set of governing equations including velocity perturbations etc. Of relevance now will be the sign and magnitude of the electrical conductivity anisotropy. Flexoelectricity has been ignored. With imposed a.c. electric fields of suitable frequency, this may be a reasonable assumption even with weak anchoring (if the dielectric constants are insensitive to the frequency of **E**). With a d.c. field, however, the conclusions of this work will be of no significance as HD may set in without threshold [29].

A conducting nematic may not support only EHD. For suitable parameters (material parameters, anchoring strengths, field directions and amplitudes, frequencies etc.), the positive feedback mechanism necessary to produce EHD may not work. Then static distortions induced by **E** may become possible [24, 25]. The equation of charge continuity is used instead of the Maxwell divergence equation to account for the effect of director perturbations on **E**. At the sample planes, the vanishing of the z component of the current will yield the boundary condition instead of (8). The dielectric anisotropy will also be operative in coupling the director and electric fields. This presents a parallel stream of investigation where both conductivity and dielectric anisotropies determine the existence of PD. Preliminary calculations show that the product of the two anisotropies plays a decisive role in influencing the results. As conductivity is a sensitive function of the a.c. frequency, it may be possible to control the occurrence of PD by varying the frequency. With the dependence of anchoring strengths on the presence of conductivity [26], the study of weak anchoring will gain a new dimension with frequency entering as an additional parameter.

The continuum theory employed in this work is strictly valid at temperatures sufficiently removed from phase transitions. Recent work [30] reports theoretical studies on the nematic–isotropic phase transition in samples of finite thickness having weak anchoring at the boundaries. Some of the phase diagrams resemble those of figures 1 and 9. Certain conclusions such as the disappearance of the bulk transition for a critical sample thickness are also strikingly similar (see definition for η_C). This accord is due to similarities in the forms of the free energy and governing equations as well as in the boundary conditions. More detailed comparisons between the two works will be attempted in future.

References

[1] De Gennes, P. G., and Prost, J., 1993, *The Physics of Liquid Crystals* (Oxford University Press).

[2] Chandrasekhar, S., 1992, *Liquid Crystals* (Cambridge University Press).

[3] Blinov, L. M., and Chigrinov, V. G., 1993, *Electrooptic Effects in Liquid Crystal Materials* (Springer Verlag).

[4] Pikin, S. A., 1991, *Structural Transformations in Liquid Crystals* (Gordon and Breach).

[5] Lonberg, F., and Meyer, R. B., 1985, *Phys. Rev. Lett.*, **55**, 718.

[6] Gooden, C., Mahmood, R., Brisbin, A., Baldwin, A., Johnson, D. L., and Neubert, M. E., 1985, *Phys. Rev. Lett.*, **54**, 1035.

[7] MEYER, R. B., 1968, *Phys. Rev. Lett.*, **22,** 918; PROST, J., and MARCEROU, J. P., 1977, *J. Phys. France*, **38,** 315; DURAND, G., 1984, *Mol. Cryst. liq. Cryst.*, **113,** 237.
[8] VISTIN, L. K., 1970, *Sov. Phys. Crystallogr.*, **15,** 514.
[9] DE JEU, W. H., GERRITSMA, C. J., VAN ZANTEN, P., and GOOSSENS, W. J. A., 1972, *Phys. Lett.*, **39A,** 335.
[10] DEULING, H. J., 1978, *Sol. St. Phys. Suppl.*, **14,** 77.
[11] BOBYLEV, YU. P., CHIGRINOV, V. G., and PIKIN, S. A., 1979, *J. Phys. Colloq. France*, **40,** C3-331; KINI, U. D., 1986 *J. Phys. France*, **47,** 693; ZIMMERMANN, W., and KRAMER, L., 1986, *Phys. Rev. Lett.*, **56,** 2655; OLDANO, C., 1986, *Phys. Rev. Lett.*, **56,** 1098; MIRALDI, E., OLDANO, C., and STRIGAZZI, A., 1986, *Phys. Rev. A*, **34,** 4348; ALLENDER, D. W., HORNREICH, R. M., and JOHNSON, D. L., 1987, *Phys. Rev. Lett.*, **59,** 2654; KINI, U. D., 1990, *Liq. Cryst.*, **7,** 185.
[12] RAPINI, A., and PAPOULAR, M., 1969, *J. Phys. Colloq. France*, **30,** C4–54; for reviews on interfacial properties, see COGNARD, J., 1982, *Mol. Cryst. liq. Cryst. Suppl.*, **1,** 1, and JEROME, B., 1991, *Rep. Progr. Phys.*, **54,** 391.
[13] ARAKELYAN, S. M., KARAYAN, A. S., and CHILINGARYAN, Y. S., 1984, *Sov. Phys. Dok.*, **29,** 202.
[14] FRISKEN, B. J., and PALFFY-MUHORAY, P., 1989, *Phys. Rev. A*, **39,** 1513; *ibid.* **40,** 6099.
[15] FRISKEN, B. J., and PALFFY-MUHORAY, P., 1989, *Liq. Cryst.*, **5,** 623; recent work in this geometry is reported in GARG, S., SAEED, S., and KINI, U. D., 1995, *Phys. Rev. E*, **51,** 5846.
[16] SEPPEN, A., MARET, G., JANSEN, A. G. M., WYDER, P., JANSSEN, J. J. M., and DE JEU, W. H., 1986, *Springer Proc. Phys.*, **11,** 18; DUNMUR, D. A., SZUMILIN, K., and WATERWORTH, T. F., 1987, *Molec. Cryst. liq. Cryst.*, **149,** 385.
[17] CUMMINS, P. G., DUNMUR, D. A., and LAIDLER, D. A., 1975, *Mol. Cryst. liq. Cryst.*, **30,** 109; BUNNING, J. D., FABER, T. E., and SHERRELL, P. L., 1981, *J. Physique*, **42,** 1175; SHERRELL, P. L., and CRELLIN, D. A., 1979, *J. Physique Colloq. Suppl.*, **40,** C3–211.
[18] ALLENDER, D. W., FRISKEN, B. J., and PALFFY-MUHORAY, P., 1989, *Liq. Cryst.*, **5,** 735.
[19] KINI, U. D., 1990, *J. Phys. France*, **51,** 529.
[20] KINI, U. D., 1995, *J. Phys. France II*, **5,** 1841.
[21] SCHAD, HP., and KELLY, S. M., 1986, *Mol. Cryst. liq. Cryst.*, **133,** 75.
[22] SCHAD, HP., and OSMAN, M. A., 1981, *J. chem. Phys.*, **75,** 880.
[23] A recent review on the subject is the article by BODENSCHATZ, E., ZIMMERMANN, W., and KRAMER, L., 1989, *J. Physique*, **49,** 1875.
[24] DEULING, H. J., and HELFRICH, W., 1974, *Appl. Phys. Lett.*, **25,** 129.
[25] DOZOV, I., BARBERO, G., PALIERNE, J. F., and DURAND, G., 1986, *Europhys. Lett.*, **1,** 563.
[26] BARBERO, G., and DURAND, G., 1990, *J. appl. Phys.*, **67,** 2678.
[27] LANDAU, L. D., and LIFSHITZ, E. M., 1984, *Electrodynamics of Continuous Media* (Pergamon Press).
[28] COHEN, G., and HORNREICH, R. M., 1990, *Phys. Rev. A*, **41,** 4402.
[29] SCHMIDT, D., SCHADT, M., and HELFRICH, W., 1972, *Z. Naturf. (a)*, **27,** 277.
[30] KOTHEKAR, N., ALLENDER, D. W., and HORNREICH, R. M., 1995, *Phys. Rev. E*, **52,** 4541.